Analysis of proton-^{9,10,11,12}Be scattering using an energy-, density-, and isospin-dependent microscopic optical potential

M. Y. H. Farag,[1,*] E. H. Esmael,[1] and H. M. Maridi[1,2,†]
[1]*Physics Department, Faculty of Science, Cairo University, Cairo, Egypt*
[2]*Physics Department, Faculty of Applied Science, Taiz University, Taiz, Yemen*
(Received 9 June 2014; revised manuscript received 27 August 2014; published 19 September 2014)

The proton elastic scattering of ^{9,10,11,12}Be isotopes at a wide energy range from 3 to 200 MeV/nucleon is analyzed using the optical model with the partial-wave expansion method. The microscopic optical potential (OP) is taken within the single-folded model. The density- and isospin-dependent M3Y-Paris nucleon-nucleon (NN) interaction is used for the real part and the NN-scattering amplitude of the high-energy approximation is used for the imaginary one. The surface contribution to the imaginary part is included. The analysis reveals that the partial-wave expansion with this microscopic OP reproduces well the basic scattering observables at energies up to 100 MeV/nucleon. For higher energies, the eikonal approximation with the same OP gives results better than the partial-wave expansion calculations. The volume integrals of the OP parts have systematic energy dependencies, and they are parameterized in empirical formulas. In addition, the volume integral's parametrizations determine the true energy dependence for the depths of the OP parts. The study of increasing the number of neutrons for a given isotope shows that the imaginary volume integrals and reaction cross sections depend on the matter radii of the scattered nuclei. Further, they are found to have larger values for the halo nucleus scattering (^{11}Be + p) than those for the scattering of their isotopes.

DOI: 10.1103/PhysRevC.90.034615 PACS number(s): 25.40.Cm, 25.60.Bx, 21.10.Gv, 24.10.Ht

I. INTRODUCTION

The optical-model potential (OP) has been developed in phenomenological and microscopic approaches to study the cross sections and analyzing powers of the scattering reaction. The phenomenological OP, in which the parameters are adjusted by fitting to scattering experimental data, is successful in a wide range of incident energies. However, it does not include nuclear structure information. In addition, it cannot give unique values of these parameters [1]. The ambiguity of the phenomenological OP arises from, in particular, the existence of a large number of optical potentials describing equally well a given set of elastic-scattering data [2].

On the other hand, the microscopic approach considers the effective potential between the nucleons. A successful microscopic OP, that is used to study the cross sections at low and intermediate incident energies, is the folding-model potential [3]. It is based on the effective nucleon-nucleon (NN) interaction and the densities of the scattered nuclei.

Recently, we studied the angular distributions for elastic-scattering cross sections and reaction cross sections for the proton elastic scattering of helium and lithium isotopes at incident energies below 160 MeV/nucleon using the optical-model analysis with the partial-wave expansion method [4,5]. The OP parts were constructed only from the single-folded potentials and their derivatives. Within the folding model, the density-independent M3Y NN interaction was used for the real part and the NN-scattering amplitude of the high-energy approximation was used for the imaginary part. The OP parts were renormalized by a few limited fitting factors to fit the data. This microscopic OP fits well the available data until 100 MeV/nucleon. The volume integrals were found to be have systematic behaviors with incident energy.

In the present work, the density and isospin dependencies are taken into consideration in the folding OP calculations because the exotic nuclei usually have nonzero isospin. In general, beryllium isotopes are light nuclei and include examples of stable, exotic, and halo nuclei. Therefore, it is interesting to study the scattering of beryllium isotopes and to analyze the effect of the halo structure. Many scattering observables, namely, reaction cross sections and angular distributions for elastic-scattering cross sections and analyzing powers, exist for the $p + ^{9,10,11,12}$Be elastic scattering over a wide range of energies from a few MeVs/nucleon up to 200 MeV/nucleon. These basic scattering observables are calculated numerically solving the Schrödinger equation by means of the optical model with the partial-wave expansion method. The real OP is constructed from the single-folded potential using the energy-, density-, and isospin-dependent M3Y-Paris NN interaction [6], whereas the so-called high-energy approximation (HEA) model is used for the imaginary OP [7–9]. The renormalization factors are chosen according to the quality of the agreement with available scattering observables and restricted by the systematic behaviors of the volume integrals. To test the ability of this OP to reproduce the data of the high-energy scattering, the cross sections at $E \geqslant 50$ MeV/nucleon are recalculated by using the eikonal approximation that based on the Glauber theory. The energy and mass dependencies of the volume integrals of the OPs are studied. The theoretical approaches are given in Sec. II, while the results of the calculations are presented in Sec. III. Summary and conclusions are given in Sec. IV.

*yehiafarag@cu.edu.eg
†h.maridi@yahoo.com

II. THEORETICAL CALCULATIONS

A. Real OP within the single-folding model

In the first order of the many-body theory, the real proton-nucleus potential is evaluated as an antisymmetrized Hartree-Fock-type potential

$$V_i = \sum_{j\in A}[\langle ij|v^{\rm D}|ij\rangle + \langle ij|v^{\rm EX}|ji\rangle], \quad (1)$$

where $v^{\rm D}$ and $v^{\rm EX}$ are the direct and exchange parts of the effective NN interaction between the incident proton i and nucleon j in the target A. The exchange term arises from the antisymmetrization between the coordinates of the incident nucleon and those of the target nucleons; see, for example, Refs. [10,12,14].

The central nucleon-nucleus potential [Eq. (1)] can be written in terms of the direct and exchange parts of the NN interaction and the nuclear density of the scattered nuclei as included in the folding model [3,10,11]. The folding model, with realistic NN interactions based upon a G matrix, is discussed by Satchler and Love [3].

Further, the symmetry (isospin dependence) term of the OP can be included in the calculation of the optical potential by considering the difference between proton (ρ_p) and neutron (ρ_n) matter densities [10,12]. Therefore, one can represent the the direct and exchange parts of the proton-nucleus potential in terms of isoscalar ($V_{\rm IS}$) and isovector ($V_{\rm IV}$) contributions as [6,13]

$$\begin{aligned} V_F(\mathbf{r}) &= V^{\rm D}(\mathbf{r}) + V^{\rm EX}(\mathbf{r}) \\ &= V^{\rm D}_{\rm IS}(\mathbf{r}) + V^{\rm D}_{\rm IV}(\mathbf{r}) + V^{\rm EX}_{\rm IS}(\mathbf{r}) + V^{\rm EX}_{\rm IV}(\mathbf{r}), \quad (2)\\ V^{\rm D}_{\rm IS(IV)}(\mathbf{r}) &= \int [\rho_p(\mathbf{r}') \pm \rho_n(\mathbf{r}')]v^{\rm D}_{00(01)}(\rho,E,s)d^3r', \quad (3)\\ V^{\rm EX}_{\rm IS(IV)}(\mathbf{r}) &= \int [\rho_p(\mathbf{r},\mathbf{r}') \pm \rho_n(\mathbf{r},\mathbf{r}')]v^{\rm EX}_{00(01)}(\rho,E,s) \\ &\quad \times j_0(k(E,r)s)d^3r', \quad (4)\end{aligned}$$

where the $+$ sign is related to the isoscalar and $-$ sign to the isovector. The isovector part of the folding OP is also known as symmetry potential. $s = |\mathbf{r}' - \mathbf{r}|$ is the distance between the proton and the nucleon in the target and $\mathbf{r}$ is the vector joining the center-of-mass of the incident proton and the target. $\rho_{p(n)}(\mathbf{r},\mathbf{r}')$ is the one-body density matrix for the protons(neutrons) in the target nucleus with $\rho_{p(n)}(\mathbf{r}) \equiv \rho_{p(n)}(\mathbf{r},\mathbf{r})$. $k(E,r)$ is the local momentum of the relative motion determined as [10,14]

$$k^2(E,r) = \frac{2\mu}{\hbar^2}[E_{\rm c.m.} - V_F(r) - V_C(r)], \quad (5)$$

where μ is the nucleon reduced mass, $E_{\rm c.m.}$ is the center-of-mass energy, and $V_F(r)$ and $V_C(r)$ are the total nuclear and Coulomb potentials, respectively.

A popular NN interaction that has been used in the folding potential is the M3Y effective NN interaction, based on the G-matrix calculations, which has two different kinds, namely the Paris [15] and the Reid NN interactions [16]. For the direct and exchange parts of NN interaction, the radial strengths of isoscalar and isovector components, $v_{00}^{\rm D(EX)}$ and $v_{01}^{\rm D(EX)}$, are defined in terms of three yukawas [15,16]. Furthermore, they are listed in simple forms in Ref. [13]. In the present work, the M3Y-Paris interaction is used.

To reproduce the basic nuclear matter properties as well as the density and energy dependencies of the nucleon OP, the NN interaction considers the energy and density dependencies as [17]

$$v^{\rm D(EX)}(\rho,E,s) = g(E)F(\rho)v^{\rm D(EX)}(s). \quad (6)$$

In the present study, we use the explicit energy and density dependencies that were introduced in Ref. [18] for the CDM3Y6 effective Paris potential as

$$g(E) = 1 - 0.003E, \quad \text{and} F(\rho) = C[1 + \alpha e^{-\beta\rho(\mathbf{r})} - \gamma\rho(\mathbf{r})], \quad (7)$$

where $C = 0.2658$, $\alpha = 3.8033$, $\beta = 1.4099$ fm^3, and $\gamma = 4.0$ fm^3.

For the density matrix, the realistic local approximation proposed in Refs. [14,19] is used:

$$\begin{aligned}\rho_q(\mathbf{r},\mathbf{r}+\mathbf{s}) &\simeq \rho_q\left(\mathbf{r}+\frac{\mathbf{s}}{2}\right)\hat{j}_1\left[k_F^q\left(\left|\mathbf{r}+\frac{\mathbf{s}}{2}\right|\right)s\right] \\ &\equiv f_q\left(\mathbf{r}+\frac{\mathbf{s}}{2}\right), \quad q \equiv p,n, \quad (8)\end{aligned}$$

where $\hat{j}_1(x) = 3j_1(x)/x = 3(\sin x - x\cos x)/x^3$. The local Fermi momentum $k_F(r)$ is defined as [19,20]

$$k_F^q(r) = \left\{\frac{5}{3\rho_q(r)}\left[\tau_q(r) - \frac{1}{4}\nabla^2\rho_q(r)\right]\right\}^{1/2}. \quad (9)$$

The kinetic energy density $\tau(r)$ can be approximated by the extended Thomas-Fermi approximation [9,21,22] as

$$\begin{aligned}\frac{\tau(\rho)}{2} \simeq \tau_q(\rho_q) &= \frac{3}{5}(3\pi^2)^{2/3}[\rho_q(r)]^{5/3} \\ &\quad + \frac{C_S|\nabla\rho_q(r)|^2}{\rho_q(r)} + \frac{\nabla^2\rho_q(r)}{3}, \quad (10)\end{aligned}$$

valid for each kind of particle $q = n,p$. C_S is the strength of the so-called Weizsäcker term representing the surface contribution to τ. For a finite fermionic system, the commonly accepted value of the Weizsäcker term is $C_S = 1/36$ [21].

The local Fermi momentum $k_F(r)$ then can be written as

$$k_F^q(r) = \left\{[3\pi^2\rho_q(r)]^{2/3} + \frac{5C_S|\nabla\rho_q(r)|^2}{3\rho_q^2(r)} + \frac{5\nabla^2\rho_q(r)}{36\rho_q(r)}\right\}^{1/2}. \quad (11)$$

Then, the direct and exchange parts of the proton-nucleus potential [Eqs. (3) and (4)] can be obtained as

$$V^{\rm D}_{\rm IS(IV)}(\mathbf{r}) = g(E)\int [\rho_p(\mathbf{r}') \pm \rho_n(\mathbf{r}')]F(\rho(\mathbf{r}'))v^{\rm D}_{00(01)}(s)d^3s \quad (12)$$

and

$$V^{\rm EX}_{\rm IS(IV)}(\mathbf{r}) = g(E)\int\left[f_p\left(\mathbf{r}+\frac{\mathbf{s}}{2}\right)\pm f_n\left(\mathbf{r}+\frac{\mathbf{s}}{2}\right)\right]\times F\left(\rho\left(\mathbf{r}+\frac{\mathbf{s}}{2}\right)\right)v^{\rm EX}_{00(01)}(s)j_0(k(E,r)s)d^3s. \quad (13)$$

For the elastic scattering, the spherical potential is radial. Therefore, the direct part of the central elastic potential [Eq. (12)] can be obtained in the following form:

$$V^{\rm D}_{\rm IS(IV)}(r) = \frac{g(E)}{2\pi^2}\int_0^\infty A_{\rm IS(IV)}(q)v^{\rm D}_{00(01)}(q)j_0(qr)q^2dq, \quad (14)$$

where $v^{\rm D}_{00(01)}(q)$ is the Fourier transform of the direct interaction $v^{\rm D}_{00(01)}(s)$ and $A_{\rm IS(IV)}(q)$ is the Fourier transform of the density profile. They are given by

$$v^{\rm D}_{00(01)}(q) = 4\pi\int_0^\infty v^{\rm D}_{00(01)}(r)j_0(qr)r^2dr, \quad (15)$$

$$A_{\rm IS(IV)}(q) = 4\pi\int_0^\infty[\rho_p(r)\pm\rho_n(r)]F(\rho(r))j_0(qr)r^2dr. \quad (16)$$

Similarly, the exchange part of the elastic potential [Eq. (13)] can be evaluated as

$$V^{\rm EX}_{\rm IS(IV)}(r) = 2\pi g(E)\int_0^\infty G_{\rm IS(IV)}(r,s)v^{\rm EX}_{00(01)}(s)\times j_0(k(E,r)s)s^2ds, \quad (17)$$

where

$$G_{\rm IS(IV)}(r,s) = \int_{-1}^{1}[f_p(y(x),s)\pm f_n(y(x),s)]F(\rho(y(x))dx, \quad (18)$$

where $f_q(y,s) = \rho_q(y)\hat{j}_1(k^q_F(y)s)$ with $q\equiv p,n$ and $y(x) = \sqrt{r^2+\frac{s^2}{4}+rsx}$. $V^{\rm EX}(r)$ includes $k(E,r)$, which is expressed by $V_F = V^{\rm D}+V^{\rm EX}$ as in Eq. (5). So, the self-consistent (local) exchange potential is calculated by an iterative procedure [22].

B. Imaginary optical potential within the high-energy approximation

The imaginary part of the OP can be calculated within the HEA model that was derived in Refs. [7,8] on the basis of the eikonal phase inherent in the optical limit of the Glauber theory. It is considered a folding potential which folds the NN-scattering amplitude and the density of the scattered nucleus. Recently, the HEA imaginary potential is used instantaneously with the real folding potential V_F to study the proton elastic scattering of light nuclei. This hybrid potential succeeds in fitting the cross-sectional experimental data at energies below 100 MeV/nucleon; see, for example, Refs. [4,5,9,23]. The imaginary OP within the HEA model is expressed as [7–9]

$$W_H(r) = -\frac{\hbar v}{(2\pi)^2}\bar{\sigma}_{NN}\int_0^\infty dqq^2j_0(qr)\rho(q)f_{NN}(q), \quad (19)$$

where v is the velocity of the nucleon-nucleus relative motion, $\rho(q)$ is the form factor corresponding to the pointlike nucleon density distribution of the nucleus, and $f_{NN}(q)$ is the amplitude of the NN scattering which can be specified in the form of a Gaussian function [7,24],

$$f_{NN}(q) = \exp\left(-q^2r_0^2/4\right), \quad (20)$$

where $r_0^2 = 0.439$ fm^2 [24] is the range parameter. $\bar{\sigma}_{NN}$ is the average over isospin total NN cross section. It has been parameterized in Refs. [24,25] as a function of energy,

$$\bar{\sigma}_{NN} = \frac{N_PN_T\sigma_{nn}+Z_PZ_T\sigma_{pp}+(Z_PN_T+N_PZ_T)\sigma_{np}}{A_PA_T}. \quad (21)$$

The pp and nn cross sections are given in (fm^2) by

$$\sigma_{pp} = \sigma_{nn} = (1.373-1.504\beta^{-1}+0.876\beta^{-2}+6.867\beta^2), \quad (22)$$

where

$$\beta = \frac{\upsilon}{c} = \sqrt{1-\left(\frac{m}{E_N+m}\right)^2} \quad (23)$$

is the ratio of the relative to the light velocities, $E_N = E/A$ is the incident energy per nucleon (in MeV), and $m = 931.494$ MeV. For the np cross section, σ_{np} is expressed in two forms as

$$\sigma_{np} = -7.067-1.818\beta^{-1}+2.526\beta^{-2}+11.35\beta \quad (24)$$

for the energy per nucleon $E_N > 10$ MeV.

For $E_N < 10$ MeV, the following expression that is given by Enge [25,26] is used:

$$\sigma_{np} = \frac{273}{(1-0.0553E_N)^2+0.35E_N}+\frac{1763}{(1+0.334E_N)^2+6.8E_N}. \quad (25)$$

C. The total optical potential

The present scattering problem considers a proton with an energy E incident upon a target with a mass number A and scattered by a central spherical optical potential $U_{\rm OP}(r)$ which can be generally written as

$$U_{\rm OP}(r) = V(r)+iW(r)+V_{\rm SO}(r)\mathbf{L}.\mathbf{S}+V_C(r), \quad (26)$$

where V, W, and $V_{\rm SO}$ are the real, imaginary, and spin-orbit parts of the OP, respectively. $V_C(r)$ is the Coulomb potential of a uniformly charged sphere of radius $1.2A^{1/3}$. The imaginary OP consists of volume and surface absorption components $[W(r) = W_v(r)+W_s(r)]$. At low incident energy, the surface absorption is too strong and $W_s(r)$ is dominant. On the other hand, the absorption is completely dominated by $W_v(r)$ at higher energies [27]. In the present calculations, the real part of the OP is constructed with the single-folded model using the density- and isospin-dependent M3Y-Paris NN interaction, whereas the volume imaginary part is taken with the HEA model. The derivative of the volume imaginary potential is added as a surface imaginary potential and the derivative of

TABLE I. $d\sigma/d\Omega$ and $A_y(\theta)$ data for proton elastic scattering of ^{9,10,11,12}Be nuclei.

Data	Scattering	Incident energy (in MeV/nucleon) [reference]
$d\sigma/d\Omega$	$p + {}^{9}$Be	3 [31], 6.0, 10.0 [32], 13 [33], 17, 25 [34], 30.3 [33], 35.2 [35], 49.4 [36], 54.7, 74.7 [37], 100.6 [38], 160 [39], 179.9 [40], and 201.4 [41]
	^{10}Be $+ p$	6, 9 [42], 12, 15 [43], 39.1 [44], and 59.3 [45]
	^{11,12} Be $+ p$	38.4 [44] and 49.3 [45] for ^{11}Be $+ p$ and 55 [46] for ^{12}Be $+ p$
$A_y(\theta)$	$p + {}^{9}$Be	8.5 [47], 11.4 [48], 13 [33], 17.8 [49], 30.3 [50], 42 [51], 74.7 [37], 100.6 [38]

the folding potential is added as a spin-orbit potential. The renormalization factors, N_R, N_I, $N_{\rm IS}$, and $N_{\rm SO}$, are introduced to fit the data. They are considered as strengths of the real, volume imaginary, surface imaginary, and spin-orbit terms of the microscopic OP, respectively. The introducing of the renormalization factors to the folding potential may be due to the dynamic polarization contributions [18]. Furthermore, the energy dependence of these renormalization factors indicates the opening of inelastic channels as the energy increases [2]. One of the aims of this work is to present energy-dependent renormalization factors.

The total microscopic optical potential can be rewritten as [5]

$$U_{OP}(r) = N_R V_F(r) + i\left[N_I W_H(r) - N_{\rm IS} r \frac{d}{dr} W_H(r)\right] - 2\lambda_\pi^2 N_{\rm SO} \frac{1}{r}\frac{d}{dr} V_F(r)\mathbf{L}.\mathbf{S} + V_C(r), \quad (27)$$

where V_F [Eq. (2)] is the real OP using the single-folded model and W_H [Eq. (19)] is the volume imaginary potential using the high-energy approximation model.

In the past decade, the microscopic density distributions for some light nuclei have been obtained using the Green's function Monte Carlo (GFMC) method. The GFMC calculation of the ground and low-lying excited states of these nuclei uses a realistic Hamiltonian containing the Argonne v18 (AV18) two-nucleon potential alone or with Illinois models (IL1-IL5) [28]. In the present work, we use the GFMC density that is based on AV18+IL2 model for ^{9,10}Be [28]. In addition, the densities of ^{11,12}Be are chosen in the form of Gaussian-oscillator (GO) distributions [29]. The parameters of the GO density are given by Ref. [4] for ^{11}Be and Ref. [30] for ^{12}Be.

Generally, the volume integral per nucleon of the spherical potential, $U(r)$, can be given by

$$J(U) = \frac{1}{A}\int U(r) d^3r = \frac{4\pi}{A}\int U(r) r^2 dr. \quad (28)$$

The values of the volume integrals are actually negative because the corresponding OP parts are attractive (negative). As usually used, the negative sign is neglected. The volume integrals of the real, imaginary, and spin-orbit parts of the OP are denoted correspondingly by J_R, J_I, and $J_{\rm SO}$. They are defined as

$$J_R = \frac{4\pi}{A}\int [N_R V_F(r)] r^2 dr, \quad (29)$$

$$J_I = \frac{4\pi}{A}\int \left[N_I W_H(r) - N_{\rm IS} r \frac{d}{dr} W_H(r)\right] r^2 dr, \quad (30)$$

and

$$J_{\rm SO} = \frac{4\pi}{A}\int \left[-2\lambda_\pi^2 N_{\rm SO} \frac{1}{r}\frac{d}{dr} V_F(r)\right] r^2 dr. \quad (31)$$

D. Method of calculations

A lot of experimental cross-sectional and analyzing-power data for $p + {}^{9,10,11,12}$Be elastic scattering exist over a wide range of energies. Some of these data in an energy range from 3 to 201.4 MeV/nucleon are considered in the present work and are listed with their references in Table I. In addition, there are several experimental values of the reaction cross sections for $p + {}^{9}$Be reaction [52,53] and unique values for ^{10,11}Be $+ p$ [53].

The microscopic optical model potential [Eq. (27)] is used in the calculations of the cross sections. The calculations of the cross sections are performed by numerical solution of the Shrödinger equation, by means of the code DWUCK4 [54], using the partial-wave expansion method. More details about these calculations can be found, for example, in Refs. [55–58].

The renormalization factors of the OP are determined by a fitting procedure of the scattering observables, which is carried out to achieve minimum χ^2. Furthermore, they must be smooth regarding energy and are chosen according to the standard behaviors of the corresponding volume integrals. The following definition of χ^2 is used:

$$\chi^2 = \frac{1}{N}\sum_{k=1}^{N}\left[\frac{\sigma_{\rm th}(\theta_k) - \sigma_{\rm ex}(\theta_k)}{\Delta\sigma_{\rm ex}(\theta_k)}\right]^2, \quad (32)$$

where $\sigma_{\rm th}(\theta_k)$ and $\sigma_{\rm ex}(\theta_k)$ are the theoretical and experimental cross sections at the angle θ_k, respectively. $\Delta\sigma_{\rm ex}(\theta_k)$ is the experimental error and N is the number of data points. The errors of the experimental data are not provided for most of the considered experimental data, so these errors can be taken as 10% of the corresponding experimental data. In addition, the visual fit must be noted by eye because the minimum χ^2 does not necessarily mean a better visual result in some cases [27].

III. RESULTS AND DISCUSSION

A. Partial-wave expansion

The calculated differential cross sections of $p + {}^{9}$Be elastic scattering are presented in Figs. 1(a) and 1(b), whereas those of ^{10,11,12}Be $+ p$ elastic scattering are presented in Figs. 1(c) and 1(d). The best-fit renormalization factors, the total reaction cross sections σ_R, and the best χ^2 values are listed in Table II.

The differential cross-sectional data for energies up to 100 MeV/nucleon are reproduced well as presented

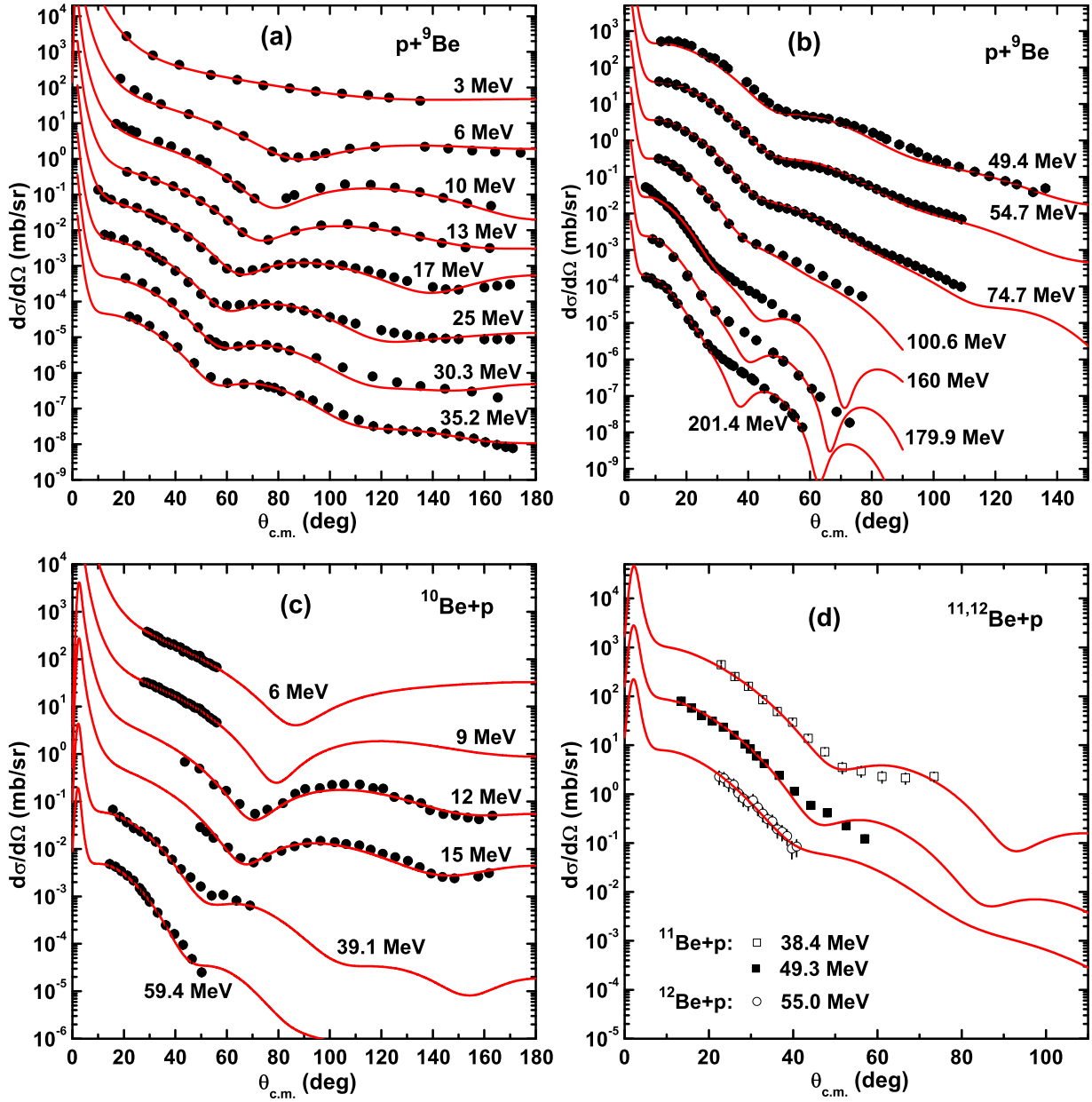

FIG. 1. (Color online) Differential cross sections for the proton elastic scattering of beryllium isotopes. The symbols represent the experimental data at different energies in MeV/nucleon and the lines represent the results of the optical model with the partial-wave expansion method of calculation. The curves and data points at the top represent true values, while the others are offset by factors of 10, 100, and so on. The experimental data are listed in Table I.

in Figs. 1(a) and 1(b) for $p + {}^{9}$Be elastic scattering and in Figs. 1(c) and 1(d) for $^{10,11,12}\mathrm{Be} + p$ elastic scattering.

For higher energies larger than 100 MeV/nucleon, more than one valley or minimum are found in the calculated differential cross sections of $p + {}^{9}$Be elastic scattering, as shown in Fig. 1(b). At 160 MeV/nucleon, the first minimum is found at around 45° and the second one at about 70°. The angular positions of these minima decrease with an increase in the incident energy. The question is arisen about the limit of using the partial-wave expansion method with the microscopic folding OP [Eq. (27)].

Generally, from Table II, the renormalization factors show systematic behaviors regarding energy, and they can be parameterized as functions of energy. More details about the energy and mass dependencies of the OP parts are given in Sec. III B.

The analyzing powers for $p + {}^{9}$Be elastic scattering are presented in Fig. 2. The partial-wave expansion method is used for these calculations. The calculated analyzing powers are with a reasonable fit of the experimental data as shown in Fig. 2.

The total nuclear reaction cross sections (σ_R) give information about the radii of the scattering nuclei and their structure. In addition, they are considered important constraints for the

TABLE II. Best-fit renormalization factors of the OP [Eq. (27)] and σ_R, obtained by fit the experimental cross-sectional and analyzing-power data for $p + {}^{9,10,11,12}$Be elastic scattering at different energies using the optical model with the partial-wave expansion method.

Nucleus	E/A (MeV)	N_R	N_I	N_{IS}	N_{SO}	χ^2	σ_R (mb)
^{9}Be	3.0	0.94	0.00	0.0013	0.22	0.98	178.9
	6.0	1.00	0.00	0.024	0.29	3.01	692.1
	10.0	1.16	0.02	0.05	0.36	6.08	614.4
	13.0	1.20	0.04	0.06	0.22	0.42	622.7
	17.0	1.28	0.09	0.07	0.15	5.59	606.7
	25.0	1.15	0.29	0.04	0.17	5.73	513.6
	30.3	1.06	0.35	0.03	0.10	7.94	449.2
	35.2	1.01	0.43	0.02	0.15	3.60	412.6
	49.4	1.09	0.56	0.00	0.12	6.22	337.1
	54.7	1.00	0.67	0.00	0.09	2.28	334.8
	74.7	1.03	0.79	0.00	0.08	5.90	290.4
	100.6	1.09	0.90	0.00	0.09	5.99	252.5
	160.0	1.58	1.00	0.00	0.16	11.49	202.4
	179.9	1.70	0.98	0.00	0.12	20.04	188.3
	201.4	1.82	0.91	0.00	0.12	20.61	170.4
^{10}Be	6.0	1.02	0.005	0.019	0.20	1.21	661.8
	9.0	1.10	0.01	0.034	0.18	1.35	615.1
	12.0	1.25	0.015	0.05	0.17	3.84	605.6
	15.0	1.23	0.03	0.067	0.17	6.09	615.7
	39.1	1.13	0.26	0.05	0.05	4.84	400.1
	59.4	1.07	0.41	0.05	0.04	3.02	329.7
^{11}Be	38.4	1.07	0.00	0.21	0.05	3.27	618.0
	49.3	1.02	0.18	0.19	0.05	17.03	544.3
^{12}Be	55.0	1.10	0.44	0.08	0.05	0.17	462.3

choice of the optical potential parameters. The calculated reaction cross sections for the proton elastic scattering of beryllium isotopes at different energies using the optical model analysis with the partial-wave expansion are presented in Fig. 3. The σ_R values obtained for the considered reactions are in agreement with the available experimental data. The σ_R decreases with an increase of the projectile incident energy for each reaction. In addition, the calculated values of σ_R are slightly greater than the corresponding experimental data at energies larger than 50 MeV/nucleon for the $p + {}^{9}$Be scattering.

Furthermore, the calculated σ_R values for the halo nucleus scattering (^{11}Be + p) are found to be larger than the calculated ones for the scattering of their isotopes ($p + {}^{9,10,12}$Be) at the same energy; see Fig. 3. In addition, σ_R for the proton elastic scattering with the ^{12}Be nucleus is larger than that for the ^{9,10}Be isotopes. It is noted that the ^{12}Be nucleus is considered as a possible two-neutron halo nucleus. Therefore, one conclude that the σ_R values depend on the rms radius of the scattered nucleus. More explanations about this result are given in Sec. III B.

B. The energy and mass dependencies of the volume integrals

The calculated volume integrals of the OPs for $p + {}^{9,10,11,12}$Be elastic scattering using the optical model analysis with the partial-wave expansion method are shown in Fig. 4. The microscopic OP is calculated using Eq. (27) and the volume integrals are calculated using Eqs. (29)–(31). The volume integrals are found to have characteristic energy

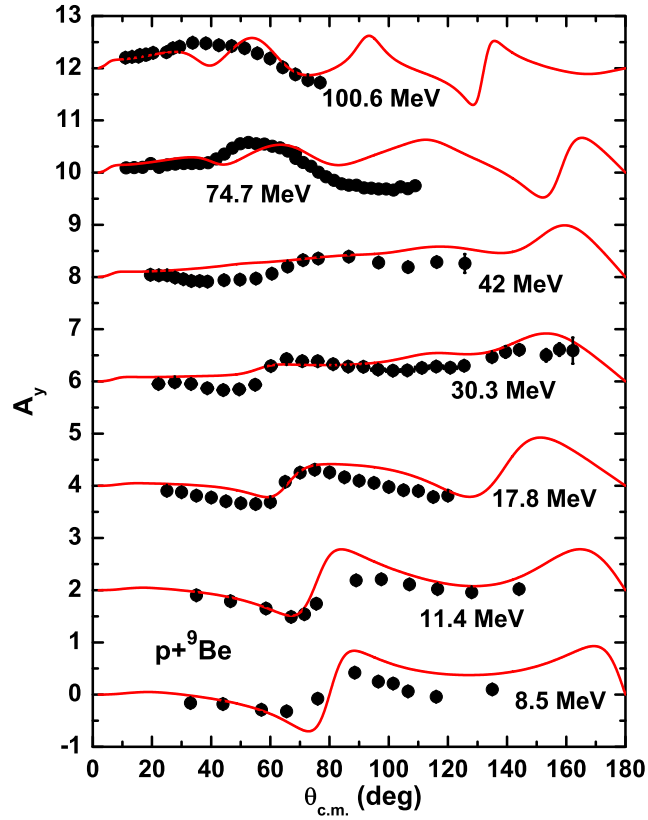

FIG. 2. (Color online) Comparisons of the experimental analyzing powers with the calculated values for $p + {}^{9}$Be elastic scattering at different energies (in MeV/nucleon). The symbols represent the data and the lines represent the results of the optical model calculation with the partial-wave expansion method. The curves and data points at the bottom represent true values, while the others by factors of 2, 4, 6, etc. The experimental data are listed in Table I.

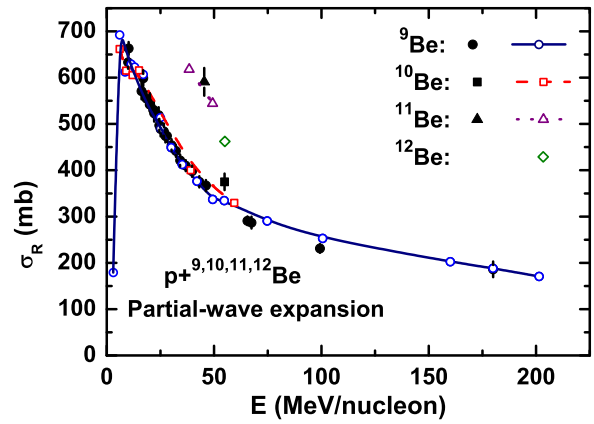

FIG. 3. (Color online) Calculated σ_R in comparison with the experimental ones for the proton elastic scattering of beryllium isotopes using the optical model with the partial-wave expansion.

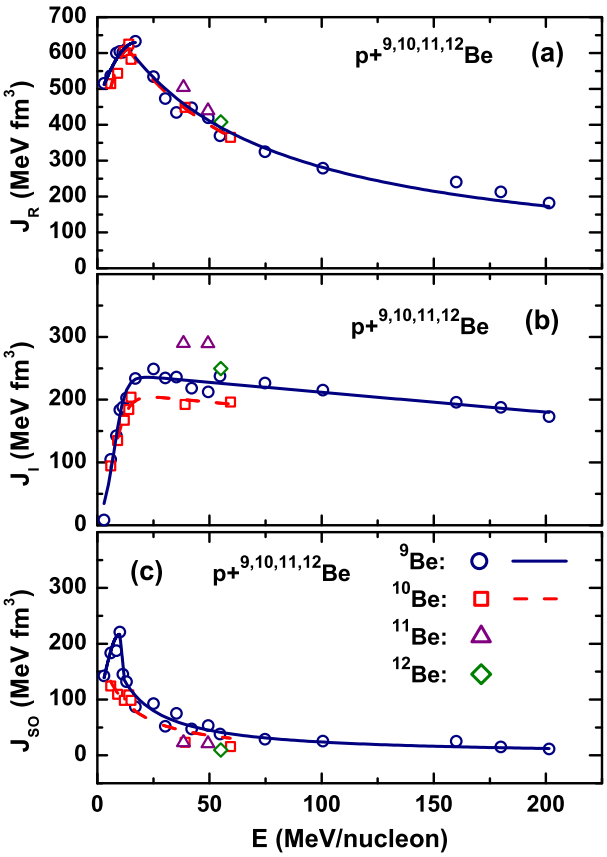

FIG. 4. (Color online) Dependence of the volume integrals on the incident energy for the proton elastic scattering of beryllium isotopes. The symbols represent the calculated volume integrals of the best-fit OPs and the lines represent the parameterized volume integrals as functions of energy.

behaviors similar to those found from the study of the proton elastic scattering of helium and lithium isotopes [5].

The $p + {}^{9,10,11,12}$Be scattering reactions have similar values of J_R. For the J_{SO}, the calculated values for the proton scattering with the stable ^{9}Be nucleus are slightly larger than those for their exotic isotopes. Clearly, the J_R and the J_{SO} increase with energy until they reach a maximum at a definite energy (denoted by E_R for J_R and E_{SO} for J_{SO}). After that, they begin to decrease with energy. E_R is found at about 15 MeV/nucleon for $p + {}^{9,10}$Be reactions and E_{SO} at about 10 MeV/nucleon for $p + {}^9$Be reaction. More experimental data at low energies are needed to determine these values for the other reactions.

Different energy parametrizations are used for the real OP or its J_R, namely, a polynomial form [27]; an exponential decay form of Perey and Buck [59], which was used, for example, in Refs. [60,61]; a logarithmic formula [62,63]; and a reciprocal formula [5]. For low energies ($E < E_R$), the rising of the real volume integral J_R was parameterized by a Gaussian formula as in Refs. [64,65]. In addition, the J_{SO} was parameterized exponentially for $E > E_{SO}$ as in Refs. [27,60,61,66]. In Ref. [5], we present a new empirical formula with two parameters only for J_R; it has a reciprocal form and is successfully applied for the proton elastic scattering of helium and lithium isotopes. In the present work, this reciprocal formula is expressed for both J_R and J_{SO}. In addition, the Gaussian parametrization is used for low energies

$$J_R(E) = \begin{cases} \frac{J_{R0}}{1+\eta_R E} & \text{for } E \geqslant E_R \\ J_{R1} \exp\left[-(E-E_R)^2/w_R^2\right] & \text{for } E \leqslant E_R. \end{cases} \quad (33)$$

Similarly

$$J_{SO}(E) = \begin{cases} \frac{J_{S0}}{1+\eta_{SO} E} & \text{for } E \geqslant E_{SO} \\ J_{S1} \exp\left[-(E-E_{SO})^2/w_{SO}^2\right] & \text{for } E \leqslant E_{SO}, \end{cases} \quad (34)$$

where $J_{k1} = J_{k0}/(1+\eta_k E_k)$ with $k = R$,SO. J_0 is the maximum value. w is the rise parameter which describes the increasing of the J_R and J_{SO} at low energies. η is the decay parameter that describes them decreasing after they reach their maximum values. In some cases, E_R and E_{SO} cannot be determined because there are no further data at low energies. Then, it can be neglected and the first lines in Eqs. (33) and (34) are only considered.

The imaginary volume integral, J_I, depends strongly on the energy because many reaction channels open at energies around the Coulomb barrier [67]. The imaginary OP takes into account the absorption of the flux in the nonelastic channels. So, it increases when a new channel is open from $J_I = 0$ below the lowest inelastic channel to a saturation value $J_I = J_{I0}$ observed at relatively high energies [65,67].

The J_I begins small at low energies and then increases rapidly up to a maximum value (J_{I0}) at a definite energy. Thereafter, the J_I values decrease linearly and slowly with increasing energy. In previous studies that were done for the proton scattering with intermediate and heavy nuclei ($A \geqslant 24$), the calculated imaginary volume integrals were saturated after they reached a maximum, as shown in Refs. [2,60,61]. However, the present study for the proton scattering with light nuclei ($A \leqslant 12$) shows that the J_I values decrease slowly after they reach a maximum. Clearly, the greatest value for J_I is found for the halo nucleus scattering ($^{11}\text{Be} + p$). In addition, the J_I value obtained for $^{10}\text{Be} + p$ elastic scattering is the smallest one, as shown in Fig. 4. The behavior of the J_I is shown to be related to the rms radius of the scattered nucleus.

There are different parametrizations for J_I: the Fermi-like parametrization that was first introduced in Ref. [68] and used in Refs. [65,69] for α scattering; the functional form of Brown and Rho [70] that was successfully applied in Refs. [27,61,66]; and the Jeukenne-Mahaux formula [71], which was applied in Ref. [60]. These formulas suggest that the J_I saturates at a maximum value, J_{I0}, at high energies. In the present work, the results show that the J_I decreases slowly and linearly with energy at high energies after it reaches the maximum. Therefore, we modify the Fermi parametrization formula to include the J_I decreasing after it reaches the maximum. It can be expressed as

$$J_I(E) = J_{I0}(1-\eta_I E)\frac{1}{1+\exp(E_I - E)/w_I} \quad (35)$$

with a maximum value J_{I0} and the global parameters: decreasing slope η_I, rise parameter w_I, and E_I.

TABLE III. Energy parametrizations of the volume integrals of the best-fit OPs for $p + {}^{9,10}$Be elastic scattering using the partial-wave expansion calculations. The parameters E and w are given in MeV, η in MeV^{-1}, and J_0 in MeV fm^3.

Reaction	J_R				J_I				J_{SO}			
	E_R	w_R	J_{R0}	η_R	E_I	w_I	J_{I0}	η_I	E_{SO}	w_{SO}	J_{S0}	η_{SO}
$p + {}^{9}$Be	17	30.78	754.9	0.0168	7.51	2.51	243.5	0.0013	10	9.48	369.7	0.1447
$p + {}^{10}$Be	14	18.23	765.0	0.0183	6.88	3.32	210.8	0.0016			213.1	0.100

The parameterized volume integrals as functions of energy for the OPs of the considered scattering reactions are shown in Fig. 4 in comparison with the calculated ones. The fitted parameters obtained for the different parametrizations are listed in Table III for J_R, J_I, and J_{SO}. It is shown that these parametrization formulas fit the calculated volume integrals well.

To study the effect of increasing the number of neutrons for a scattered isotope, the dependence of the imaginary volume integrals and the reaction cross sections on the mass number of beryllium isotopes are presented in Fig. 5. They are presented in comparison with the experimental rms matter radii that are given in Ref. [72]. J_I and σ_R are presented in two different energy groups (37 ± 2 and 54 ± 5 MeV/nucleon) as shown in Figs. 5(a) and 5(b). The first group includes $p + {}^{9}$Be at 35.2 MeV/nucleon, ^{10}Be $+ p$ at 39.1 MeV/nucleon, and ^{11}Be $+ p$ at 38.4 MeV/nucleon. The second group contains $p + {}^{9}$Be at 54.7 MeV/nucleon, ^{10}Be $+ p$ at 59.4 MeV/nucleon, ^{11}Be $+ p$ at 49.3 MeV/nucleon, and ^{12}Be $+ p$ at 55 MeV/nucleon. It is shown that the behaviors of the J_I and σ_R are similar for the different energy groups for $p + {}^{9,10,11,12}$Be elastic scattering. Clearly, the calculated values of the J_I and σ_R depend strongly on the rms radius of the isotope. More experimental data are needed to estimate the mass dependence of the volume integral parametrizations.

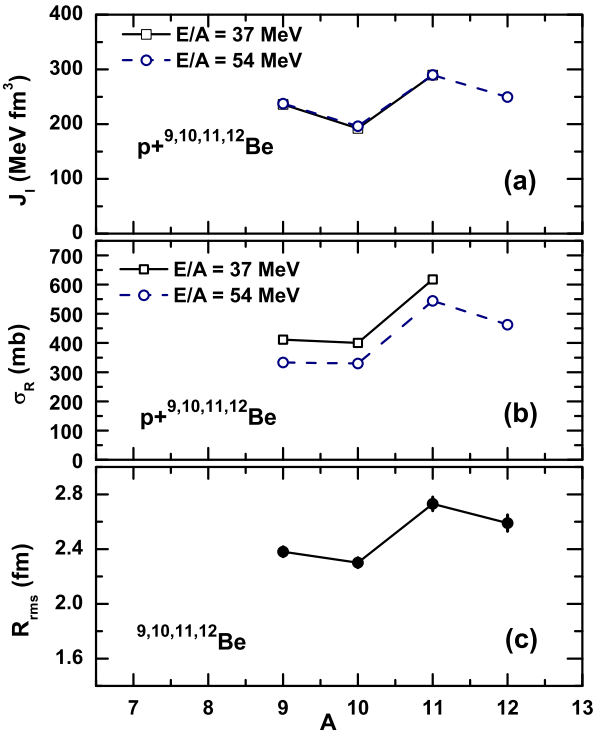

FIG. 5. (Color online) Mass dependence of the imaginary volume integrals and σ_R for the proton elastic scattering of beryllium isotopes. They are compared with the experimental matter rms radii given in Ref. [72].

From these parameterized volume integrals, one can determine the energy dependence of the renormalization factors and the local energy-dependent OP as shown in Ref. [73]. The parameterized renormalization factors as a function in energy can be calculated from joining Eqs. (33), (34), and (35) with Eqs. (29), (30), and (31).

C. The eikonal approximation

From the partial-wave expansion calculations, it is found that the cross-sectional data are not reproduced well at relatively high energies larger than 100 MeV/nucleon as shown in Sec. III A. This may be due to the limit of using the partial-wave expansion method with the single-folded OP. At these high energies, the wave function will oscillate rapidly and the calculations of scattering wave functions for each partial wave become more complicated. Instead of the partial-wave expansion, a relativistic correction such as the eikonal approximation is useful.

The eikonal approximation is based on the optical limit of the Glauber theory [74]. The Glauber model is reasonable for energies of hundreds MeV and higher. However, at low energies, the modified Glauber models are used [7,25,75–77]. By use of the eikonal approximation one avoids the calculation of scattering wave functions by solving numerically the Shrödinger equation for each partial wave.

Then, the differential cross sections of the elastic scattering and reaction cross sections of $p + {}^{9}$Be at energies larger than 50 MeV/nucleon are recalculated using the eikonal approximation with the DWEIKO code [78]. The microscopic OP [Eq. (27)] is used in the calculation to test its ability of reproducing the cross-sectional data at high energies.

The calculated differential cross sections of $p + {}^{9}$Be elastic scattering using the eikonal approximation are presented in Fig. 6 in comparison with the results of the optical model code with the partial-wave expansion method. The renormalization factors, the total reaction cross sections σ_R, and the best χ^2 values for the eikonal approximation calculations are listed in Table IV.

It is clear that the eikonal approximation model gives good agreement with the data at energies larger than 50 MeV/nucleon over all the angular range. The minima or

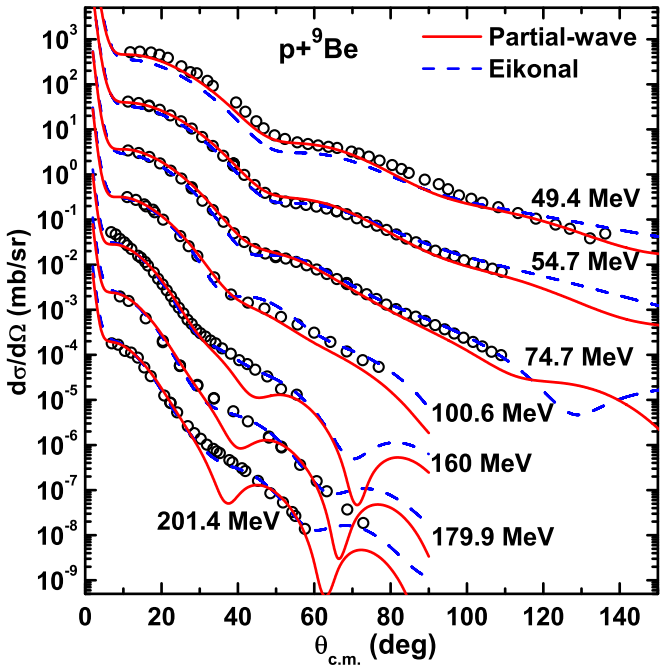

FIG. 6. (Color online) Differential cross sections for $p + {}^{9}$Be elastic scattering. The symbols represent the experimental data at different energies in MeV/nucleon. The solid lines represent the results of the partial-wave expansion calculations, whereas the dashed lines represent the results of the eikonal approximation calculations. The curves and data points at the top represent true values, while the others are offset by factors of 10, 100, and so on.

valleys that are shown in the angular distribution using the partial-wave analysis are disappeared.

The calculated reaction cross sections for $p + {}^{9}$Be elastic scattering at different energies are presented in Fig. 7. The calculated values of σ_R using the eikonal approximation give good agreement with the experimental data, better than those results of the partial-wave expansion.

Table IV show that the renormalization factors have systematic behaviors with energy. Figure 8 shows that the volume integrals of the best-fit OPs using the eikonal approximation in comparison with their parametrizations [Eqs. (33), (34), and (35)]. In addition, they are compared with the partial-wave expansion calculation. Because we use the eikonal approximation for energies larger than 50 MeV/nucleon, the first lines in Eqs. (33) and (34) are considered only for J_R and J_{SO}. Also, the linear relation in Eq. (35) that describes the J_I decreasing is only considered.

TABLE IV. The same as Table II but by use of the eikonal approximation for $p + {}^{9}$Be elastic scattering at energies $E \geqslant$ 50 MeV/nucleon.

E/A (MeV)	N_R	N_I	N_{IS}	N_{SO}	χ^2	σ_R (mb)
49.4	0.96	0.55	0.07	0.05	18.81	308.6
54.7	0.88	0.60	0.06	0.05	3.72	290.7
74.7	0.80	0.76	0.05	0.07	2.44	257.4
100.6	0.95	0.92	0.05	0.10	5.10	235.0
160.0	1.37	1.12	0.01	0.07	2.77	187.1
179.9	1.24	1.09	0.01	0.02	115.0[a]	176.3
201.4	1.53	0.95	0.00	0.03	4.26	150.7

[a] χ^2 value is large but the visual fit is acceptable.

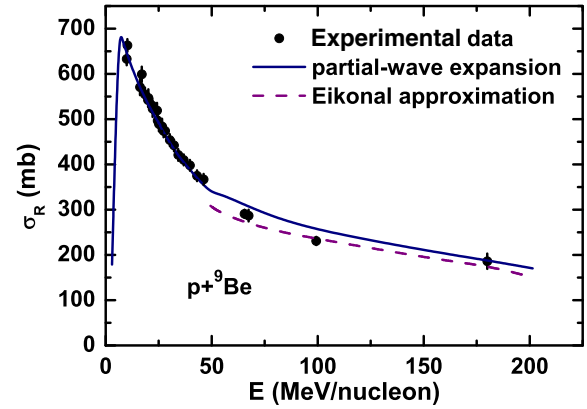

FIG. 7. (Color online) Calculated σ_R for $p + {}^{9}$Be elastic scattering using the optical model with the partial-wave expansion in comparison with eikonal approximation results for high energies.

From the comparison between the partial-wave expansion and the eikonal approximation in Fig. 8, the two methods give similar behaviors for the volume integrals, but they have

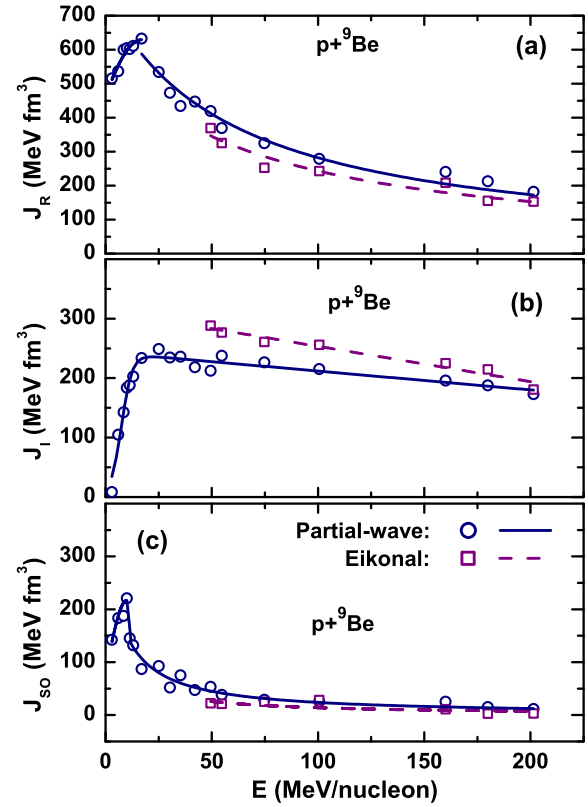

FIG. 8. (Color online) Dependence of the volume integrals on the incident energy for $p + {}^{9}$Be elastic scattering. The symbols represent the calculated volume integrals and the lines represent the parameterized volume integrals as functions of energy.

TABLE V. Energy parametrizations of the volume integrals of the best-fit OPs for $p + {}^{9}$Be elastic scattering using the eikonal approximation. The parameters η are given in MeV and J_0 in MeV fm^3.

J_R		J_I		J_{SO}	
J_{R0}	η_R	J_{I0}	η_I	J_{S0}	η_{SO}
593.2	0.0144	313.0	0.0019	153.8	0.100

different values. The calculated values of the J_R and J_{SO} using the eikonal approximation are found to be less than those use the partial-wave expansion. For J_I, the calculated values by use of the eikonal approximation are larger than those using the partial-wave expansion method.

IV. SUMMARY AND CONCLUSIONS

Microscopic analysis was performed for the proton elastic scattering of beryllium isotopes over a wide energy range from 3 to 201.4 MeV/nucleon. The basic scattering observables (angular distributions for elastic-scattering cross sections and analyzing powers, and reaction cross sections) were calculated using the optical model with the partial-wave expansion. The OP parts were constructed from the single-folded potential using the density- and isospin-dependent M3Y-Paris NN interaction for the real part and the NN-scattering amplitude within the high-energy approximation model for the imaginary part. The derivatives of the real and volume imaginary parts of the OP were added as spin-orbit and surface-imaginary OPs, respectively.

The partial-wave expansion calculation using this microscopic OP successfully reproduces the experimental observables at energies until to 100 MeV/nucleon. Above this energy value, some minima appear in the calculated angular distribution of the elastic-scattering cross sections. The halo nuclei scattering has value of σ_R larger than that for the scattering of their isotopes, which indicates to the dependence of σ_R on the rms radius of the scattering nucleus. The disagreement of the cross sections at relatively high energies may need a relativistic correction. Therefore, the eikonal approximation method was used and the cross sections were recalculated for energies that greater than 50 MeV/nucleon. It is used with the same OP and compared with the partial-wave expansion method. The eikonal approximation reproduces the differential cross-sectional data well at energies larger than 100 MeV/nucleon, and the minima were disappeared. Furthermore, the σ_R values obtained using the eikonal approximation are smaller than those use the partial-wave expansion method and give the best agreement with the data of the high-energy scattering.

The volume integrals have systematic behaviors for the energy and mass dependencies. The J_R increases with increasing energy until it reaches a maximum at a definite value of energy, E_R. Thereafter, with increasing incident energy, the J_R decreases reciprocally. The behavior of the J_{SO} is similar to the J_R. On the other hand, the J_I increases rapidly up to the maximum value (J_{I0}). After that, the J_I decreases linearly with a small slope. The J_I for the halo nucleus scattering has a value larger than that for the other isotopes. The study of increasing the number of neutrons for the scattered isotope shows a direct relation between the J_I and the rms radius of the isotope. Different energy parametrizations were applied for the volume integrals. The reciprocal formula was used for the J_R and J_{SO} and the Fermi-like parametrization was modified and applied for the J_I. They successfully parameterized the calculated volume integrals. From these parametrization, a local E-dependent OP can be obtained with parameterized renormalization factors as a function in energy. More experimental data for the exotic nuclei scattering should be done at low energies to give the correct energy and mass dependence of the OPs and their volume integrals.

[1] P. E. Hodgson, Rep. Prog. Phys. **34**, 765 (1971).
[2] M. E. Brandan and G. R. Satchler, Phys. Rep. **285**, 143 (1997).
[3] G. R. Satchler and W. G. Love, Phys. Rep. **55**, 183 (1979).
[4] M. Y. H. Farag, E. H. Esmael, and H. M. Maridi, Eur. J. Phys. A **48**, 154 (2012).
[5] M. Y. H. Farag, E. H. Esmael, and H. M. Maridi, Phys. Rev. C **88**, 064602 (2013).
[6] D. T. Khoa, E. Khan, G. Colò, and N. Van Giai, Nucl. Phys. A **706**, 61 (2002).
[7] P. Shukla, Phys. Rev. C **67**, 054607 (2003).
[8] V. K. Lukyanov, E. V. Zemlyanaya, and K. V. Lukyanov, Phys. At. Nucl. **69**, 240 (2006).
[9] K. V. Lukyanov, V. K. Lukyanov, E. V. Zemlyanaya, A. N. Antonov, and M. K. Gaidarov, Eur. J. Phys. A **33**, 389 (2007).
[10] G. L. Thomas, B. C. Sinha, and F. Duggan, Nucl. Phys. A **203**, 305 (1973).
[11] B. Sinha and S. A. Moszkdwski, Phys. Lett. B **81**, 289 (1979).
[12] F. A. Brieva and J. R. Rook, Nucl. Phys. A **291**, 317 (1977).
[13] D. T. Khoa, W. von Oertzen, and A. A. Ogloblin, Nucl. Phys. A **602**, 98 (1996).
[14] B. Sinha, Phys. Rep. **20**, 1 (1975).
[15] N. Anantaraman, H. Toki, and G. F. Bertsch, Nucl. Phys. A **398**, 269 (1983).
[16] G. Bertsch, J. Borysowicz, H. McManus, and W. G. Love, Nucl. Phys. A **284**, 399 (1977).
[17] D. T. Khoa and W. von Oertzen, Phys. Lett. B **304**, 8 (1993).
[18] D. T. Khoa, G. R. Satchler, and W. von Oertzen, Phys. Rev. C **56**, 954 (1997).
[19] X. Campi and A. Bouyssy, Phys. Lett. B **73**, 263 (1978).
[20] J. W. Negele and D. Vautherin, Phys. Rev. C **5**, 1472 (1972).
[21] P. Ring and P. Schuck, *The Nuclear Many-Body Problem* (Springer-Verlag, New York, 1980), p. 542.
[22] D. T. Khoa, W. von Oertzen, and H. G. Bohlen, Phys. Rev. C **49**, 1652 (1994).
[23] V. K. Lukyanov, E. V. Zemlyanaya, K. V. Lukyanov, D. N. Kadrev, A. N. Antonov, M. K. Gaidarov, and S. E. Massen, Phys. Rev. C **80**, 024609 (2009).

[24] P. Shukla, arXiv:nucl-th/0112039.
[25] S. K. Charagi and S. K. Gupta, Phys. Rev. C **41**, 1610 (1990); **46**, 1982 (1992).
[26] H. A. Enge, *Introduction to Nuclear Physics* (Addison-Wesley, Reading, MA, 1966).
[27] A. J. Koning and J. P. Delaroche, Nucl. Phys. A **713**, 231 (2003).
[28] S. C. Pieper, K. Varga, and R. B. Wiringa, Phys. Rev. C **66**, 044310 (2002).
[29] G. D. Alkhazov *et al.*, Nucl. Phys. A **712**, 269 (2002).
[30] S. Ilieva *et al.*, Nucl. Phys. A **875**, 8 (2012).
[31] D. H. Loyd and W. Haeberli, Nucl. Phys. A **148**, 236 (1970).
[32] F. W. Bingham, M. K. Brussel, and J. D. Steben, Nucl. Phys. **55**, 265 (1964).
[33] H. J. Votava, T. B. Clegg, E. J. Ludwig, and W. J. Thompson, Nucl. Phys. A **204**, 529 (1973).
[34] D. G. Montague, R. K. Cole, P. S. Lewis, C. N. Waddell, and D. L. Hendrie, Nucl. Phys. A **199**, 433 (1973).
[35] E. Fabrici, S. Micheletti, M. Pignanelli, F. G. Resmini, R. De Leo, G. D'Erasmo, and A. Pantaleo, Phys. Rev. C **21**, 844 (1980).
[36] N. M. Clarke, E. J. Burge, D. A. Smith, and J. C. Dore, Nucl. Phys. A **157**, 145 (1970).
[37] L. J. de Bever *et al.*, Nucl. Phys. A **579**, 13 (1994).
[38] H. Seifert, Ph.D. thesis, University of Maryland, 1990 (unpublished).
[39] P. G. Roos and N. S. Wall, Phys. Rev. **140**, B1237 (1965).
[40] S. Dixit *et al.*, Phys. Rev. C **43**, 1758 (1991).
[41] H. Seifert *et al.*, Phys. Rev. C **47**, 1615 (1993).
[42] K. T. Schmitt *et al.*, Phys. Rev. C **88**, 064612 (2013).
[43] D. L. Auton, Nucl. Phys. A **157**, 305 (1970).
[44] V. Lapoux *et al.*, Phys. Lett. B **658**, 198 (2008).
[45] M. D. Cortina-Gil *et al.*, Phys. Lett. B **401**, 9 (1997).
[46] A. A. Korsheninnikov *et al.*, Phys. Lett. B **343**, 53 (1995).
[47] L. Rosen, J. E. Brolley Jr., M. L. Gursky, and L. Stewart, Phys. Rev. **124**, 199 (1961).
[48] L. Rosen, J. E. Brolley Jr., and L. Stewart, Phys. Rev. **121**, 1423 (1961).
[49] D. J. Baugh, J. A. R. Griffith, and S. Roman, Nucl. Phys. **83**, 481 (1966).
[50] D. L. Watson, J. Lowe, J. C. Dore, R. M. Craig, and D. J. Baugh, Nucl. Phys. A **92**, 193 (1967).
[51] T. A. Cahill, J. R. Richardson, and R. P. Haddock, Phys. Rev. **144**, 932 (1966).
[52] R. F. Carlson, At. Data Nucl. Data Tables **63**, 93 (1996).
[53] A. de Vismes *et al.*, Nucl. Phys. A **706**, 295 (2002).
[54] P. D. Kunz and E. Rost, in *Computational Nuclear Physics*, edited by K. Langanke *et al.* (Springer-Verlag, New York, 1993), Vol. 2, p. 88.
[55] J. V. Lepore, Phys. Rev. **79**, 137 (1950).
[56] L. I. Schiff, *Quantum Mechanics* (McGraw-Hill, New York, 1949).
[57] A. Messiah, *Quantum Mechanics* (North-Holland, Amsterdam, 1961).
[58] E. H. Auerbach, Comput. Phys. Commun. **15**, 165 (1978).
[59] F. G. Perey and B. Buck, Nucl. Phys. **32**, 353 (1962).
[60] O. V. Bespalova, E. A. Romanovsky, and T. I. Spasskaya, J. Phys. G: Nucl. Part. Phys. **29**, 1193 (2003).
[61] B. Morillon and P. Romain, Phys. Rev. C **70**, 014601 (2004); **76**, 044601 (2007).
[62] W. T. H. Van Oers and H. Haw, Phys. Lett. B **45**, 227 (1973).
[63] A. Nadasen, S. Balaji, J. Brace, K. A. G. Rao, P. G. Roos, P. Schwandt, and J. T. Ndefru, Phys. Rev. C **66**, 064605 (2002).
[64] P. Mohr, Phys. Rev. C **61**, 045802 (2000).
[65] P. Demetriou, C. Grama, and S. Goriely, Nucl. Phys. A **707**, 253 (2002).
[66] X. Li and C. Cai, Nucl. Phys. A **801**, 43 (2008).
[67] U. Atzrott, P. Mohr, H. Abele, C. Hillenmayer, and G. Staudt, Phys. Rev. C **53**, 1336 (1996).
[68] E. Somorjai *et al.*, Astron. Astrophys. **333**, 1112 (1998).
[69] Z. Fülöp *et al.*, Phys. Rev. C **64**, 065805 (2001).
[70] G. E. Brown and M. Rho, Nucl. Phys. A **372**, 397 (1981).
[71] J. P. Jeukenne and C. Mahaux, Nucl. Phys. A **394**, 445 (1983).
[72] I. Tanihata *et al.*, Phys. Lett. B **206**, 592 (1988).
[73] M. Y. H. Farag, E. H. Esmael, and H. M. Maridi, Eur. J. Phys. A **50**, 106 (2014).
[74] R. J. Glauber, in *Lectures in Theoretical Physics*, edited by W. E. Brittin and G. L. Dunham (Interscience, New York, 1959), Vol. 1, p. 315.
[75] A. Vitturi and F. Zardi, Phys. Rev. C **36**, 1404 (1987).
[76] M. Y. H. Farag, Eur. Phys. J. A **12**, 405 (2001).
[77] M. H. Cha, Phys. Rev. C **46**, 1026 (1992)
[78] C. A. Bertulani, C. M. Campbell, and T. Glasmacher, Comput. Phys. Commun. **152**, 317 (2003).